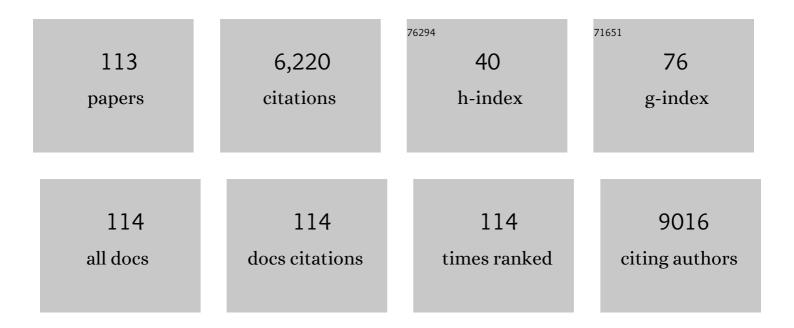
Sun Hee Choi

List of Publications by Year in descending order

Source: https://exaly.com/author-pdf/523337/publications.pdf Version: 2024-02-01



#	Article	IF	CITATIONS
1	Microwave-assisted metal-ion attachment for ex-situ zirconium doping into hematite for enhanced photoelectrochemical water splitting. Renewable Energy, 2022, 189, 694-703.	4.3	17
2	Synchronized effect of in-situ Ti doping and microwave-assisted SiOx hole transport channel on ZnFe2O4 nanocoral arrays for efficient photoelectrochemical water splitting. Applied Surface Science, 2022, 592, 153212.	3.1	13
3	Influence of ZnO Magnetron Sputtering on Controlled Buildout of Zirconium-Doped ZnFe ₂ O ₄ /Fe ₂ O ₃ Heterojunction Photoanodes for Photoelectrochemical Water Splitting. ACS Applied Energy Materials, 2022, 5, 915-929.	2.5	9
4	Efficient charge transfers in hematite photoanode integrated by fluorine and zirconia co-doping for photoelectrochemical water splitting. Chemical Engineering Journal, 2022, 446, 136957.	6.6	11
5	Detonated growth and functionalization of iron (III) oxyhydroxide nanorod array templates via microwave-assisted synthesis for photoelectrochemical water splitting. Applied Surface Science, 2022, 596, 153609.	3.1	7
6	Enhanced charge transfer with tuning surface state in hematite photoanode integrated by niobium and zirconium co-doping for efficient photoelectrochemical water splitting. Applied Catalysis B: Environmental, 2022, 315, 121538.	10.8	30
7	Microwave-assisted surface attachment of aluminium ions on <i>in situ</i> diluted titanium-doped hematite photoanodes for efficient photoelectrochemical water-splitting. Sustainable Energy and Fuels, 2022, 6, 3056-3067.	2.5	7
8	Lowering the onset potential of Zr-doped hematite nanocoral photoanodes by Al co-doping and surface modification with electrodeposited Co–Pi. Journal of Colloid and Interface Science, 2021, 581, 751-763.	5.0	23
9	Selfâ€ŧemplated fabrication of 2-D dual nanoarchitecture Zn1-xCdxS porous nanosheet and ZnO nanorod for photoelectrochemical hydrogen production. Applied Surface Science, 2021, 539, 148267.	3.1	14
10	Rational design of interface refining through Ti ⁴⁺ /Zr ⁴⁺ diffusion/doping and TiO ₂ /ZrO ₂ surface crowning of ZnFe ₂ O ₄ nanocorals for photoelectrochemical water splitting. Catalysis Science and Technology, 2021, 11, 3141-3152.	2.1	13
11	A systematic study of post-activation temperature dependence on photoelectrochemical water splitting of one-step synthesized FeOOH CF photoanodes with erratically loaded ZrO ₂ . Sustainable Energy and Fuels, 2021, 5, 3414-3427.	2.5	18
12	Magnetron sputtering strategy for Zr-Fe2O3 nanorod photoanode fabricated from ZrOx/β-FeOOH nanorods for photoelectrochemical water splitting. Applied Surface Science, 2021, 549, 149233.	3.1	27
13	Topotactic and Self-Templated Fabrication of Zn _{1–<i>x</i>} Cd <i>_x</i> Se Porous Nanobelt–ZnO Nanorod for Photoelectrochemical Hydrogen Production. ACS Applied Materials & Interfaces, 2021, 13, 29450-29460.	4.0	10
14	Effect of low-temperature solvothermal route on controlled growth mechanism of Se rich-ZnSe(en)0.5 templates for ZnO NR-Zn1-xCdxSe photoelectrodes. Applied Catalysis B: Environmental, 2021, 298, 120621.	10.8	9
15	Solid-phase arsenic speciation using XANES: preservation of arsenic species for reliable and accurate environmental risk assessment. International Journal of Environmental Analytical Chemistry, 2020, , 1-18.	1.8	3
16	Effect of Sn-self diffusion via H2 treatment on low temperature activation of hematite photoanodes. Catalysis Science and Technology, 2020, 10, 4245-4255.	2.1	3
17	Response to Comment on "Dry reforming of methane by stable Ni–Mo nanocatalysts on single-crystalline MgO― Science, 2020, 368, .	6.0	1
18	Porous Zn1-xCdxS nanosheets/ZnO nanorod heterojunction photoanode via self-templated and cadmium ions exchanged conversion of ZnS(HDA)0.5 nanosheets/ZnO nanorod. Chemical Engineering Journal, 2020, 402, 126153.	6.6	27

#	Article	IF	CITATIONS
19	Transparent Zirconium-doped Hematite Nanocoral Photoanode via In-Situ Diluted Hydrothermal Approach for Efficient Solar Water Splitting. Chemical Engineering Journal, 2020, 390, 124504.	6.6	27
20	Dry reforming of methane by stable Ni–Mo nanocatalysts on single-crystalline MgO. Science, 2020, 367, 777-781.	6.0	372
21	Synthesis of transparent Zr-doped ZnFe2O4 nanocorals photoanode and its surface modification via Al2O3/Co–Pi for efficient solar water splitting. Applied Surface Science, 2020, 513, 145528.	3.1	29
22	An effective strategy to promote hematite photoanode at low voltage bias via Zr4+/Al3+ codoping and CoOx OER co-catalyst. Electrochimica Acta, 2019, 319, 444-455.	2.6	17
23	Mixed Transition Metal Oxide with Vacancy-Induced Lattice Distortion for Enhanced Catalytic Activity of Oxygen Evolution Reaction. ACS Catalysis, 2019, 9, 7099-7108.	5.5	85
24	Improved Interfacial Charge Transfer Dynamics and Onset Shift in Nanostructured Hematite Photoanodes via Efficient Ti ⁴⁺ /Sn ⁴⁺ Heterogeneous Self-Doping Through Controlled TiO ₂ Underlayers. ACS Sustainable Chemistry and Engineering, 2019, 7, 6947-6958.	3.2	25
25	Facile synthesis of Bi2S3 nanosheet/Zr:Fe2O3 nanorod heterojunction: Effect of Ag interlayer on the change transport and photoelectrochemical stability. Journal of Industrial and Engineering Chemistry, 2019, 70, 311-321.	2.9	12
26	Hybrid Microwave Annealing for Fabrication of More Efficient Semiconductor Photoanodes for Solar Water Splitting. ACS Sustainable Chemistry and Engineering, 2019, 7, 944-949.	3.2	15
27	Superlattice Formation of Crystal Water in Layered Double Hydroxides for Longâ€Term and Fast Operation of Aqueous Rechargeable Batteries. Advanced Energy Materials, 2018, 8, 1703572.	10.2	17
28	Metalâ€Free Artificial Photosynthesis of Carbon Monoxide Using Nâ€Đoped ZnTe Nanorod Photocathode Decorated with Nâ€Đoped Carbon Electrocatalyst Layer. Advanced Energy Materials, 2018, 8, 1702636.	10.2	42
29	Enhanced Photocatalytic Degradation of Organic Pollutants and Inactivation of <i>Listeria monocytogenes</i> by Visible Light Active Rh–Sb Codoped TiO ₂ Nanorods. ACS Sustainable Chemistry and Engineering, 2018, 6, 4302-4315.	3.2	44
30	Insights into the enhanced photoelectrochemical performance of hydrothermally controlled hematite nanostructures for proficient solar water oxidation. Dalton Transactions, 2018, 47, 4076-4086.	1.6	9
31	Effect of tetravalent dopants on hematite nanostructure for enhanced photoelectrochemical water splitting. Applied Surface Science, 2018, 427, 1203-1212.	3.1	51
32	Highly self-diffused Sn doping in α-Fe ₂ O ₃ nanorod photoanodes initiated from β-FeOOH nanorod/FTO by hydrogen treatment for solar water oxidation. Nanoscale, 2018, 10, 22560-22571.	2.8	47
33	Activation of a highly oriented columnar structure of ZnFe2O4 for photoelectrochemical water splitting: Orchestrated effects of two-step quenching and Sn4+ diffusion. Solar Energy Materials and Solar Cells, 2018, 187, 207-218.	3.0	29
34	A multitude of modifications strategy of ZnFe2O4 nanorod photoanodes for enhanced photoelectrochemical water splitting activity. Journal of Materials Chemistry A, 2018, 6, 12693-12700.	5.2	52
35	Enhanced photoelectrochemical performance of internally porous Au-embedded α-Fe ₂ O ₃ photoanodes for water oxidation. Chemical Communications, 2017, 53, 4278-4281.	2.2	10
36	Surfactant and TiO 2 underlayer derived porous hematite nanoball array photoanode for enhanced photoelectrochemical water oxidation. Chemical Engineering Journal, 2017, 320, 81-92.	6.6	21

#	Article	IF	CITATIONS
37	Sodium ontaining Spinel Zinc Ferrite as a Catalyst Precursor for the Selective Synthesis of Liquid Hydrocarbon Fuels. ChemSusChem, 2017, 10, 4764-4770.	3.6	89
38	Tunable Photoluminescence across the Visible Spectrum and Photocatalytic Activity of Mixed-Valence Rhenium Oxide Nanoparticles. Journal of the American Chemical Society, 2017, 139, 15088-15093.	6.6	33
39	Fabrication of A/R-TiO 2 composite for enhanced photoelectrochemical performance: Solar hydrogen generation and dye degradation. Applied Surface Science, 2017, 426, 833-843.	3.1	49
40	Carbon dioxide Fischer-Tropsch synthesis: A new path to carbon-neutral fuels. Applied Catalysis B: Environmental, 2017, 202, 605-610.	10.8	230
41	Photocatalytic activity of electron-deficient and porous WO3 nanoparticles derived from thermal oxidation of bulk WC particles. Journal of Photochemistry and Photobiology A: Chemistry, 2016, 330, 37-43.	2.0	3
42	Oxygen-Intercalated CuFeO ₂ Photocathode Fabricated by Hybrid Microwave Annealing for Efficient Solar Hydrogen Production. Chemistry of Materials, 2016, 28, 6054-6061.	3.2	113
43	Trade-off between Zr Passivation and Sn Doping on Hematite Nanorod Photoanodes for Efficient Solar Water Oxidation: Effects of a ZrO ₂ Underlayer and FTO Deformation. ACS Applied Materials & Interfaces, 2016, 8, 19428-19437.	4.0	51
44	Sn/Be Sequentially co-doped Hematite Photoanodes for Enhanced Photoelectrochemical Water Oxidation: Effect of Be2+ as co-dopant. Scientific Reports, 2016, 6, 23183.	1.6	75
45	Subnanometer Cobalt-Hydroxide-Anchored N-Doped Carbon Nanotube Forest for Bifunctional Oxygen Catalyst. ACS Applied Materials & Interfaces, 2016, 8, 1571-1577.	4.0	67
46	Onset potential behavior in α-Fe ₂ O ₃ photoanodes: the influence of surface and diffusion Sn doping on the surface states. Physical Chemistry Chemical Physics, 2016, 18, 2495-2509.	1.3	96
47	A Synergistic Effect of Surfactant and ZrO2 Underlayer on Photocurrent Enhancement and Cathodic Shift of Nanoporous Fe2O3 Photoanode. Scientific Reports, 2016, 6, 32436.	1.6	17
48	Photoelectrochemical, impedance and optical data for self Sn-diffusion doped Fe 2 O 3 photoanodes fabricated at high temperature by one and two-step annealing methods. Data in Brief, 2015, 5, 796-804.	0.5	16
49	Selective Formation of HÃǥg Iron Carbide with gâ€C ₃ N ₄ as a Sacrificial Support for Highly Active Fischer–Tropsch Synthesis. ChemCatChem, 2015, 7, 3488-3494.	1.8	46
50	Tree branch-shaped cupric oxide for highly effective photoelectrochemical water reduction. Nanoscale, 2015, 7, 7624-7631.	2.8	90
51	Exploiting the dynamic Sn diffusion from deformation of FTO to boost the photocurrent performance of hematite photoanodes. Solar Energy Materials and Solar Cells, 2015, 141, 71-79.	3.0	48
52	Activation of Hematite Photoanodes for Solar Water Splitting: Effect of FTO Deformation. Journal of Physical Chemistry C, 2015, 119, 3810-3817.	1.5	108
53	Bifunctional TiO ₂ underlayer for α-Fe ₂ O ₃ nanorod based photoelectrochemical cells: enhanced interface and Ti ⁴⁺ doping. Journal of Materials Chemistry A, 2015, 3, 5007-5013.	5.2	90
54	Fine-Tuning Pulse Reverse Electrodeposition for Enhanced Photoelectrochemical Water Oxidation Performance of α-Fe ₂ O ₃ Photoanodes. Journal of Physical Chemistry C, 2015, 119, 5281-5292.	1.5	30

#	Article	IF	CITATIONS
55	Electrochemically Induced Structural Transformation in a γ-MnO ₂ Cathode of a High Capacity Zinc-Ion Battery System. Chemistry of Materials, 2015, 27, 3609-3620.	3.2	788
56	Defective ZnFe ₂ O ₄ nanorods with oxygen vacancy for photoelectrochemical water splitting. Nanoscale, 2015, 7, 19144-19151.	2.8	183
57	Role of Graphene Oxide as a Sacrificial Interlayer for Enhanced Photoelectrochemical Water Oxidation of Hematite Nanorods. Journal of Physical Chemistry C, 2015, 119, 19996-20002.	1.5	29
58	Awakening Solar Waterâ€5plitting Activity of ZnFe ₂ O ₄ Nanorods by Hybrid Microwave Annealing. Advanced Energy Materials, 2015, 5, 1401933.	10.2	95
59	New Insight into Copper Sulfide Electrocatalysts for Quantum Dot-Sensitized Solar Cells: Composition-Dependent Electrocatalytic Activity and Stability. ACS Applied Materials & Interfaces, 2014, 6, 22078-22087.	4.0	109
60	Highly Active and Stable Hydrogen Evolution Electrocatalysts Based on Molybdenum Compounds on Carbon Nanotube–Graphene Hybrid Support. ACS Nano, 2014, 8, 5164-5173.	7.3	531
61	Equilibria, kinetics, and spectroscopic analyses on the uptake of aqueous arsenite by two-line ferrihydrite. Environmental Technology (United Kingdom), 2014, 35, 251-261.	1.2	17
62	Sequestration of arsenate from aqueous solution using 2-line ferrihydrite: equilibria, kinetics, and X-ray absorption spectroscopic analysis. Environmental Earth Sciences, 2014, 71, 3307-3318.	1.3	9
63	Mechanisms of enhanced sulfur tolerance on samarium (Sm)-doped cerium oxide (CeO ₂) from first principles. Physical Chemistry Chemical Physics, 2014, 16, 10727-10733.	1.3	16
64	Thickness dependent magnetic properties of (111)-oriented Co 0.8 Fe 2.2 O 4 thin film grown by pulsed laser deposition. Thin Solid Films, 2014, 571, 62-68.	0.8	10
65	Fabrication of graphene-based electrode in less than a minute through hybrid microwave annealing. Scientific Reports, 2014, 4, 5492.	1.6	76
66	(111)-Oriented Co0.8Fe2.2O4+δ thin film grown by pulsed laser deposition: structural and magnetic properties. Journal of Materials Science, 2013, 48, 6960-6969.	1.7	10
67	Enhancing the catalytic activity of Pt nanoparticles using poly sodium styrene sulfonate stabilized graphene supports for methanol oxidation. Journal of Materials Chemistry A, 2013, 1, 3489.	5.2	73
68	A highly efficient transition metal nitride-based electrocatalyst for oxygen reduction reaction: TiN on a CNT–graphene hybrid support. Journal of Materials Chemistry A, 2013, 1, 8007.	5.2	126
69	Photocatalytic selective oxidation of the terminal methyl group of dodecane with molecular oxygen over atomically dispersed Ti in a mesoporous SiO2 matrix. Green Chemistry, 2013, 15, 3387.	4.6	10
70	Photocatalytic synthesis of oxygenated hydrocarbons from diesel fuel for mobile deNOx application. Journal of Catalysis, 2013, 302, 58-66.	3.1	2
71	Selective deposition of Pt onto supported metal clusters for fuel cell electrocatalysts. Nanoscale, 2012, 4, 6461.	2.8	16
72	In-situ synthesis, local structure, photoelectrochemical property of Fe-intercalated titanate nanotube. International Journal of Hydrogen Energy, 2012, 37, 11081-11089.	3.8	12

#	Article	IF	CITATIONS
73	Active size-controlled Ru catalysts for selective CO oxidation in H2. Applied Catalysis B: Environmental, 2012, 127, 129-136.	10.8	17
74	Light-Induced Cleaning of CdS and ZnS Nanoparticles: Superiority to Annealing as a Postsynthetic Treatment of Functional Nanoparticles. Journal of Physical Chemistry C, 2012, 116, 15427-15431.	1.5	3
75	Synthesis, electronic property and photocatalytic applications of mesoporous cobalt-doped ZnS and ZnO nanoplates. Applied Catalysis A: General, 2012, 427-428, 106-113.	2.2	26
76	Palladium–nickel alloys loaded on tungsten carbide as platinum-free anode electrocatalysts for polymer electrolyte membrane fuel cells. Chemical Communications, 2011, 47, 5792.	2.2	62
77	Interactions Between Tetrahydrothiophene (THT) and Silver Species in AgNa-Y. Journal of Nanoscience and Nanotechnology, 2010, 10, 203-210.	0.9	1
78	Structural characterization and effect of dehydration on the Ni-doped titanate nanotubes. Catalysis Today, 2009, 146, 230-233.	2.2	8
79	Luminescence and local structure of Mn-doped ZnS hybrid crystal with two-dimensional platelet morphology. Chemical Physics Letters, 2009, 468, 253-256.	1.2	5
80	Observation of slowly decreasing molecular oscillations in ultrathin liquid films using X-ray reflectivity. European Physical Journal: Special Topics, 2009, 167, 163-169.	1.2	0
81	High Electrochemical Li Intercalation in Titanate Nanotubes. Journal of Physical Chemistry C, 2009, 113, 14034-14039.	1.5	15
82	Band Gap Tailored Zn(Nb1â^'xVx)2O6 Solid Solutions as Visible Light Photocatalysts. Journal of Physical Chemistry C, 2009, 113, 17824-17830.	1.5	23
83	N-Doped ZnS Nanoparticles Prepared through an Inorganicâ^'Organic Hybrid Complex ZnS·(piperazine) _{0.5} . Journal of Physical Chemistry C, 2009, 113, 20445-20451.	1.5	27
84	Enhanced Photocatalytic Hydrogen Production from Waterâ^'Methanol Solution by Nickel Intercalated into Titanate Nanotube. Journal of Physical Chemistry C, 2009, 113, 8990-8996.	1.5	72
85	Transesterification of Dimethylcarbonate and Phenol Over Silica Supported TiO2 and Ti-MCM 41 Catalysts: Structure Insensitivity. Catalysis Letters, 2008, 123, 115-122.	1.4	9
86	Influence of Sn content on PtSn/C catalysts for electrooxidation of C1–C3 alcohols: Synthesis, characterization, and electrocatalytic activity. Applied Catalysis B: Environmental, 2008, 82, 89-102.	10.8	261
87	Topotactic synthesis of mesoporous ZnS and ZnO nanoplates and their photocatalytic activity. Journal of Catalysis, 2008, 254, 144-155.	3.1	144
88	Indium induced band gap tailoring in AgGa1â^'xInxS2 chalcopyrite structure for visible light photocatalysis. Journal of Chemical Physics, 2008, 128, 154717.	1.2	51
89	Location and State of Pt in Platinized CdS/TiO ₂ Photocatalysts for Hydrogen Production from Water under Visible Light. Journal of Physical Chemistry C, 2008, 112, 17200-17205.	1.5	188
90	Phase and photoelectrochemical behavior of solution-processed Fe2O3 nanocrystals for oxidation of water under solar light. Applied Physics Letters, 2008, 93, .	1.5	56

#	Article	IF	CITATIONS
91	Implementation of Enhanced Quick-scan Technique for Time-Resolved XAFS Experiment at PLS. AIP Conference Proceedings, 2007, , .	0.3	0
92	Structural Characterization of AgGaS2-type Photocatalysts for Hydrogen Production from Water Under Visible Light. AIP Conference Proceedings, 2007, , .	0.3	4
93	AgGaS2-type photocatalysts for hydrogen production under visible light: Effects of post-synthetic H2S treatment. Journal of Solid State Chemistry, 2007, 180, 1110-1118.	1.4	36
94	Metal–insulator transition induced by electronic and structural modulations in oxygen-deficient perovskite-type TbBaCo2O5.5. Physica Status Solidi (B): Basic Research, 2006, 243, 1813-1822.	0.7	14
95	Electronic states and local structures of Cu ions in electrodeposited thin films of Cu and Cu2O from X-ray absorption spectra. Physica Status Solidi (B): Basic Research, 2006, 243, 1791-1801.	0.7	3
96	Correlation between displacive-type ferroelectricity and electronic density of states near the Fermi level in SrBi2Ta2O9. Physica Status Solidi (B): Basic Research, 2005, 242, 899-908.	0.7	3
97	Correlation between the metal-insulator transition and the electronic density of states near the Fermi level in oxygen-deficient perovskite-type NdBaCo2O5.5. Physica Status Solidi (B): Basic Research, 2005, 242, 1422-1430.	0.7	4
98	The formation of precipitates in the ZnCoO system. Europhysics Letters, 2005, 72, 76-82.	0.7	30
99	X-ray Absorption Fine Structure Analysis of the Local Environment of Fe in Fe/Alâ~'MFI. Journal of Physical Chemistry B, 2004, 108, 8970-8975.	1.2	39
100	X-ray Absorption Fine Structure Characterization of the Local Structure of Fe in Feâ^'ZSM-5. Journal of Physical Chemistry B, 2003, 107, 11843-11851.	1.2	87
101	Mn-Promoted Ni/Al2O3 Catalysts for Stable Carbon Dioxide Reforming of Methane. Journal of Catalysis, 2002, 209, 6-15.	3.1	124
102	Reply to Comment on "Quantitative Analysis of Tiâ^'Oâ^'Si and Tiâ^'Oâ^'Ti Bonds in Tiâ^'Si Binary Oxides by the Linear Combination of XANESâ€: Journal of Physical Chemistry B, 2001, 105, 6274-6274.	1.2	1
103	XAFS study on Mn-Ni/Al2O3catalyst for carbon dioxide reforming of methane. Journal of Synchrotron Radiation, 2001, 8, 596-598.	1.0	4
104	Linear combination of XANES for quantitative analysis of Ti–Si binary oxides. Journal of Synchrotron Radiation, 2001, 8, 163-167.	1.0	13
105	XAFS Study of Tin Modification of Supported Palladium Catalyst for 1,3-Butadiene Hydrogenation in the Presence of 1-Butene. Journal of Catalysis, 2000, 193, 176-185.	3.1	41
106	Characterization of Pd/C and Cu Catalysts for the Oxidation of Methane to a Methanol Derivative. Journal of Catalysis, 2000, 194, 33-44.	3.1	22
107	Quantitative Analysis of Tiâ^'Oâ^'Si and Tiâ^'Oâ^'Ti Bonds in Tiâ^'Si Binary Oxides by the Linear Combination of XANES. Journal of Physical Chemistry B, 2000, 104, 8670-8678.	1.2	73
108	Active States of Pd and Cu in Carbon-Supported Wacker-Type Catalysts for Low-Temperature CO Oxidation. Journal of Physical Chemistry B, 2000, 104, 5586-5594.	1.2	52

#	Article	IF	CITATIONS
109	Effects of Pt Precursors on Hydrodechlorination of Carbon Tetrachloride over Pt/Al2O3. Journal of Catalysis, 1997, 166, 284-293.	3.1	48
110	XAFS Characterization of Pt–Mo Bimetallic Catalysts for CO Hydrogenation. Journal of Catalysis, 1997, 167, 364-371.	3.1	28
111	XAFS characterization of supported PdCl2â^'CuCl2 catalysts for CO oxidation. Reaction Kinetics and Catalysis Letters, 1996, 57, 227-236.	0.6	17
112	Supported PdCl2CuCl2 catalysts for carbon monoxide oxidation II. XAFS characterization. Applied Catalysis B: Environmental, 1996, 7, 199-212.	10.8	31
113	Hydrodechlorination of Carbon Tetrachloride over Pt/MgO. Journal of Catalysis, 1996, 161, 790-797.	3.1	69